APPLIED ORGANOMETALLIC CHEMISTRY, VOL. 6, 533–536 (1992)

Structural study of self-assembled monolayers of ferrocenylalkanethiols on gold by angle-resolved X-ray photoelectron spectroscopy

Satoshi Shogen,* Masahiro Kawasaki,* Toshihiro Kondo,† Yukari Satoh† and Kohei Uosaki†

*Institute for Electronics Science and †Department of Chemistry, Faculty of Science, Hokkaido University, Sapporo 060, Japan

An angle-resolved X-ray photoelectron spectroscopic study has been performed on structures of self-assembling systems, viz ferrocenylthiols on a gold (111) crystal. The angular dependence of the intensities of photoemission reveals that ferrocenyl groups are on the outermost layer, separated from the gold substrate by hydrocarbon chains of the thiol groups

Keywords: Photoelectron spectroscopy, gold substrate, ferrocenylthiol, self-assembling system

1 INTRODUCTION

Recently, much attention has been paid to the preparation and characterization of organized mono- and multi-molecular layers on solid surfaces because these systems provide surfaces with special functionalities.[1] The distance between particular functional groups and a solid surface can be controlled in these systems, which may thus be considered as building blocks of molecular electronics devices.

Although the Langmuir–Blodgett method has been the most popular technique for forming the molecular layers, the layers formed by this method adsorb only physically on a solid substrate and, therefore, are usually unstable. On the other hand, in the case of the self-assembling method of organometallic compounds, molecules with a reactive functional group and a long hydrocarbon chain chemisorb on a solid surface by forming covalent bonds with atoms of the surface, and a highly organized structure is established due to the intermolecular cohesion interaction between alkyl chains.[2–5]

One of the most interesting self-assembling systems investigated so far is a ferrocenylalkanethiol monolayer on gold.[6–10] In this system, the thiol group reacts with the gold atoms forming covalent bonds, while the ferrocene groups are supposed to act as an electron donor. Actually it was proved that the electron transfer between a ferrocene group and a gold electrode takes place in solution, even when a long methylene group separates the ferrocene group from the gold electrode. Although the methylene group inhibits the direct electron transfer between Fe(II)/Fe(III) in solution and the gold electrode, the ferrocene group of the monolayer mediates the electron transfer only from the gold electrode to Fe(III), achieving unidirectional electron transfer.[9]

To understand these electron transfer properties quantitatively, information on the distance between a ferrocene group and a gold electrode is essential. We have applied angle-resolved X-ray photoemission spectroscopy to studying structures of self-assembled monolayers of 6-ferrocenylhexanethiol (C_6Fc) and 11-ferrocenylundecanethiol ($C_{11}Fc$) on gold substrates in vacuum. In this paper, we confirm that the ferrocene group is situated on the outer side of the layer and the distance between Fe and Au is larger in $C_{11}Fc$ than that in C_6Fc.

2 EXPERIMENTAL

Synthesized ferrocenylalkanethiols in hexane solution were adsorbed onto an Au (111) substrate that was prepared by vacuum deposition on cleaned glass. Details have been described previously.[8] In brief, a ferrocene group of an as-adsorbed molecule is in a reduced state [Fe(II)]. The oxidized form [Fe(III)] was obtained by electrochemical oxidation in 1 mol dm^{-3} perchloric acid ($HClO_4$) solution.

Angle-resolved X-ray photoelectron spectra were measured with a spectrometer (Vacuum

0268–2605/92/060533–04 $07.00

Received 16 March 1992
Accepted 28 May 1992

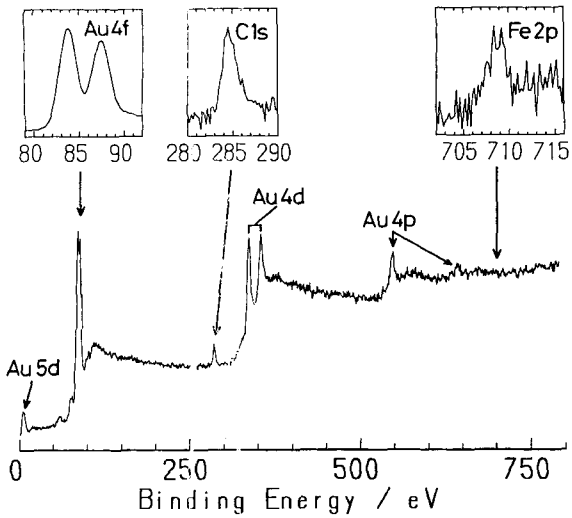

Figure 1 X-ray photoelectron spectrum of 6-ferrocenylhexanethiol on a gold (111) substrate with resolution of 3.0 eV. Insets show Au_{4f}, C_{1s}, and Fe_{2p} signals with a resolution of 2.1 eV. Accumulation numbers are 3 for Au_{4f} and C_{1s}, and 20 for Fe_{2p}. Polar emission angle $\theta = 40°$.

Generator, ADES-400), in which a 150° spherical sector analyzer with a 50 mm mean radius is moved in one plane around a specimen. The angular resolution of the analyzer is about 2°. Al K_α radiation (1486.6 eV) was used for excitation. The energy resolution of the analyzer was 3.0 eV for a wide energy scan and 2.1 eV for a narrow energy scan. Measurements of the weak Fe_{2p} signal were performed by repeating the scan approximately 20 times. The polar emission angle θ is defined as the taking-off angle of photoelectrons from a surface. Polar angle rotations are about an axis perpendicular to the plane of X-ray incidence and electron emission. The polar angle scanning was performed from 10° to 80° by rotation of the analyzer and the sample holder. Base pressure in the analyzer chamber was 3×10^{-9} Torr.

3 RESULTS

Figure 1 shows an example of the XPS spectrum ($\theta = 40°$) for C_6Fc adsorbed on Au (111). Au, Fe, S and C were observed. Among the several peaks of Au, Au_{4f} at a binding energy (BE) of 82–89 eV was measured with a narrow energy scan as shown in the inset. The Fe_{2p} signal at BE = 708 eV was so weak that the inset shows the profile after 20 repetitions of the narrow energy scan. The ratios of intensities thus obtained were calibrated for atomic sensitivities of 3.8 for Fe_{2p}, 0.25 for C_{1s}, 0.35 for S_{2p} and 1.9 for Au_{4f}.[11] The [S]/[Fe] ratio was 1.3 ± 0.3, which was in fair agreement with the expected value, 1. The [Fe]/[Au] ratios are plotted as a function of $1/\sin\theta$ in Fig. 2.

For the strong carbon signal the [C]/[Fe] ratio was found to be 35 ± 16 for the C_6Fc/Au sample, which is much larger than the expected value, 6. This was also the case for the $C_{11}Fc$ on Au. The ratio was 35 ± 6 for the $C_{11}Fc$/Au sample. Although the substrate was in the high-vacuum chamber, the outermost layer was already contaminated by hydrocarbons during the sample preparation procedure. The ratio [C]/[Au] was measured as a function of angle θ. With θ increasing from 10° to 70°, the value decreased typically from 4 to 1.7. This angular dependence of the [C]/[Au] ratio shows the carbon species are on the surface of the Au substrate. The surface layers are shown schematically in Fig. 3.

4 DISCUSSION

The basic mechanism of surface sensitivity enhancement at grazing emission angles has been given by Fadley.[12] In brief, the mean free path for inelastic scattering of photoelectrons Λ_e is taken to be a constant and independent of emission angle. In this case, the mean depth of no-loss

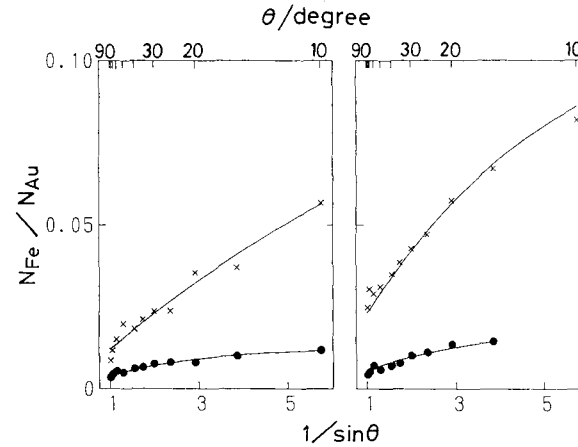

Figure 2 Angle dependence of the [Fe]/[Au] intensity ratio for (left) oxidative species of 6-ferrocenylhexanethiol (●) and 11-ferrocenylhexanethiol (×) on a gold (111) substrate and (right) reductive species on Au. Solid lines are optimized curves of Eqn [4] with the parameters of Table 1.

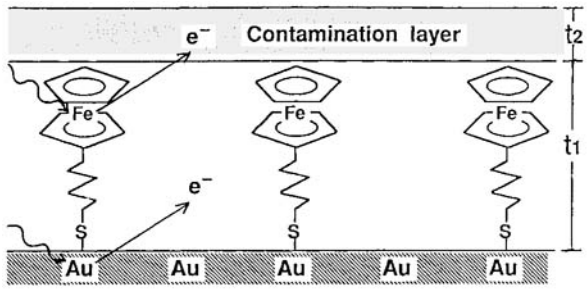

Figure 3 Schematic diagram of surface layers on Au: t_1 and t_2 denote thicknesses of carbon overlayer and ferrocene carbon layers, respectively. Wavy lines represent incident X-rays and e^- is an ejected photoelectron.

photoelectron emission as measured perpendicular to the surface is exactly equal to Λ_e for the normal emission, or $\theta = 90°$, but it decreases as $\Lambda_e \sin\theta$ for the non-normal emission. Polar scans of photoelectron intensity are thus expected to exhibit varying degrees of surface sensitivity. The photoelectrons travel to the surface, during which time they can be inelastically attenuated according to $\exp(-z/\Lambda_e \sin\theta)$, where θ is the internal propagation angle and $z/\sin\theta$ is the path length to the surface.

In a quantitative discussion of such variations of peak intensities with polar angle θ, we consider a case for a semi-infinite substrate with an attenuating overlayer of thickness t. As first discussed by Fraser *et al.*,[13] the intensity of the substrate with photoelectron energy E_k is angle-dependent:

$$N_k(\theta) = N_k^\infty \exp(-t/\Lambda_e(E_k)\sin\theta) \qquad [1]$$

$$N_k^\infty = AS\Lambda_e/d$$

where N_k^∞ is the total intensity without the attenuating overlayer, A a slit function of the XPS instrument, S the mean surface density of atoms, d the mean separation between layers of density S, and $\Lambda_e(E_k)$ an attenuation length in the substrate.

Note that there is no θ dependence in N_k^∞ within this simple model. Its origin lies in the fact that the effective emitting depth is $\Lambda_e \sin\theta$, while the effective specimen surface area is $A_0/\sin\theta$ where A_0 is an aperture area. The effective specimen volume at any θ is thus the product of the two, in which the $\sin\theta$ factors cancel. This behavior is expected to hold as long as θ is not made so small that the edges of the specimen lie within the aperture A_0.

If we assume the sandwich structure of Fig. 3, i.e. (Au substrate with infinite thickness) + (ferrocenyl compound with thickness t_1) + (carbon contamination overlayer with thickness t_2), then the intensity of the monolayered Fe atoms is also attenuated by the outermost carbon contamination layer with thickness t_2:

$$N_{Fe}(\theta) = N_{Fe}^\infty(\theta)\exp(-t_2/\Lambda_e'(E_{Fe})\sin\theta), \qquad [2]$$

$$N_{Fe}^\infty(\theta) = AS_{Fe}/\sin\theta,$$

where Λ_e' is an attenuation length in the carbon overlayer. N_{Fe}^∞ is angle-dependent because Fe atoms are monolayered.

Since the intensity of the Au substrate is also attenuated by the carbon layers of both ferrocenyl compound (t_1) and contamination compound (t_2),

$$N_{Au}(\theta) = N_{Au}^\infty \exp\{-(t_1 + t_2)/\Lambda_e'(E_{Au})\sin\theta\} \qquad [3]$$

$$N_{Au}^\infty = AS_{Au}\Lambda_e(E_{Au})/d$$

It follows that the intensity ratio $R(\theta)$ is given by:

$$R(\theta) \equiv N_{Fe}(\theta)/N_{Au}(\theta) \qquad [4]$$

$$= (a/\sin\theta)\exp(T/\sin\theta)$$

$$a = (S_{Fe}/S_{Au})[d_{Au}/\Lambda_e(E_{Au})]$$

$$T = t_1/\Lambda_e'(E_{Au}) - t_2[1/\Lambda_e'(E_{Fe}) - 1/\Lambda_e'(E_{Au})]$$

The best-fit procedures for N_{Fe}/N_{Au} are shown by the curves in Fig. 2. The parameters a and T thus obtained are tabulated in Table 1. These parameters are almost the same for the oxidative and reductive molecules. This fact suggests that the iron–gold distance in the oxidative type is not so different from that in the reductive one.

Figure 3 shows a schematic diagram of the surface-adsorbed species. When t_2 due to the

Table 1 Optimized parameters of Eqn [4] for angular distributions of photoelectron signals

	Coefficients of Eqn [4]			
	Oxidative		Reductive	
Molecule	T	a	T	a
C_6Fc	−0.148	0.0047	−0.144	0.0065
$C_{11}Fc$	−0.042	0.012	−0.090	0.025
$a(C_{11}Fc)/a(C_6Fc)$		2.6		3.8

carbon-contaminated layer is taken as the same for both C_6Fc and $C_{11}Fc$, one can calculate the difference of t_1 values for $C_{11}Fc$ and C_6Fc from the coefficient T of Table 1:

$$t_1(C_{11}) - t_1(C_6) = [T(C_{11}) - T(C_6)]\Lambda_e'(E_{Au}) \quad [5]$$

where $t_1(C_{11})$ and $t_1(C_6)$ are the effective thickness of the hydrocarbon chains of $C_{11}Fc$ and C_6Fc, respectively. $T(C_{11})$ and $T(C_6)$ are T values of Eqn [4] for $C_{11}Fc$ and C_6Fc.

According to the universal curve of the escape depth for solid samples, $\Lambda_{ev}'(E_{Au} = 1403\,eV)$ is estimated to be 18 Å (1.8 nm). However, electrochemical measurements showed that the ratio of the number of adsorbed molecules to that of surface gold atoms is *ca* 1:3.[8] One terminal sulfur atom of C_6Fc is bonded to three Au atoms when a monolayer of C_6Fc is formed, and hence the effective escape depth Λ_e' should be much larger than that of the universal curve for a solid specimen. One may estimate the effective $\Lambda_e'(E_{Au})$ would be three times 18 Å, i.e. 54 Å. Using this value and T from Table 1, the difference $t_1(C_{11})$–$t_1(C_6)$ is obtained to be 2.9–5.7 Å for oxidative and reductive species. These values are in reasonable agreement with the difference of the chain lengths of C_{11} and C_6 hydrocarbons, i.e. the thickness t_1 of C_6Fc ($C_{11}Fc$) is estimated to be 7 Å (13 Å) by using the tetrahedral angle and all-*trans* structure of the hydrocarbon chains.

Acknowledgement This work is partly supported by Grants-in-Aid from the Ministry of Education, Science and Culture, Japan (Nos 02205003, 03205003).

REFERENCES

1. Ulman, A *An Introduction to Ultrathin Organic Films from Langmuir–Blodgett to Self-Assembling*, Academic Press, San Diego, 1991
2. Sagiv, J *J. Am. Chem. Soc.*, 1980, 102: 92
3. Bain, C D, Troughton, E B, Tao, Y T, Evall, J, Whitesides, G M and Nuzzo, R G *J. Am. Chem. Soc.*, 1989, 111: 321
4. Porter, M D, Bright, T B, Allara, D L and Chidsey, C E D *J. Am. Chem. Soc.*, 1987, 109: 3559
5. Finklea, H O, Avery, S, Lynch, M and Furtsch, T *Langmuir*, 1987, 3: 409
6. Chidsey, C E D, Bertozzi, C R, Putvinski, T M and Mujsce, A M *J. Am. Chem. Soc.*, 1990, 112: 4301
7. Hickman, J J, Ofer, D, Laibinis, P E, Whitesides, G M and Wrighton, M S *Science*, 1991, 252: 688
8. Uosaki, K, Sato, Y and Kita, H *Langmuir*, 1991, 7: 1510
9. Uosaki, K, Sato, Y and Kita, H *Electrochim. Acta*, 1991, 36: 1799
10. Shimazu, K, Yagi, I, Sato, Y and Uosaki, K *Langmuir*, 1992, 8: 1385
11. Wagner, C D, Riggs, W M, Davis, L E, Moulder, J F and Muilenberg, G E *Handbook of X-Ray Photoelectron Spectroscopy*, Perkin-Elmer Corp., Minnesota, 1979
12. Fadley, C S, *Surf. Sci.*, 1984, 16: 275
13. Fraser, W A, Florio, J V, Delgass, W N and Robertson, W D *Surf. Sci.*, 1973, 36: 661